Elongated σ-Borane versus σ-Borane in Pincer-POP-Osmium Complexes

Miguel A. Esteruelas,[†] Israel Fernández,[‡] Cristina García-Yebra,[†] Jaime Martín,[†] and Enrique Oñate[†]*

[†]Departamento de Química Inorgánica, Instituto de Síntesis Química y Catálisis Homogénea (ISQCH), Centro de Innovación en Química Avanzada (ORFEO-CINQA), Universidad de Zaragoza-CSIC, 50009 Zaragoza, Spain

[‡]Departamento de Química Orgánica I, Facultad de Ciencias Químicas, Centro de Innovación en Química Avanzada (ORFEO-CINQA), Universidad Complutense de Madrid, 28040 Madrid, Spain

Supporting Information Placeholder

ABSTRACT: Square pyramidal metal fragments $OsHX\{\kappa^3\text{-}P,O,P\text{-}[xant(P^iPr_2)_2]\}$ (X = Cl, H; $xant(P^iPr_2)_2$ = 9,9-dimethyl-4,5-bis(diisopropylphosphine)xanthene) coordinate the B-H bond of boranes *trans* to the ligand X. As a consequence, elongated σ-borane and σ-borane pincer-POP-osmium complexes have been isolated and fully characterized. The interaction between the metal fragment and the coordinated B-H has been analyzed as a function of X, from spectroscopic, X-ray diffraction, and theoretical points of view. The dinuclear complex $[(Os(H\cdots H)\{\kappa^3\text{-}P,O,P\text{-}[xant(P^iPr_2)_2]\})_2(\mu\text{-}Cl)_2][BF_4]_2$ (**3**) reacts with catecholborane (HBcat) and pinacolborane (HBpin) to give the elongated σ-borane derivative $OsHCl(\eta^2\text{-}H\text{-}BR_2)\{\kappa^3\text{-}P,O,P\text{-}[xant(P^iPr_2)_2]\}$ (BR_2 = Bcat (**4**), Bpin (**5**)), H_2, FBR_2, and BF_3. The elongated σ-borane character of **4** and **5** is supported by X-ray diffraction analysis and DFT-optimized structures of both compounds, which show distances between the coordinated B and H atoms of the borane in the range 1.6-1.7 Å. AIM analysis of **4** reveals a triangular topology for the OsHB unit involving Os-B, Os-H, and B-H bond critical points and a ring critical point. In contrast to **3**, the reaction of the tetrahydride complex $OsH_4\{\kappa^3\text{-}P,O,P\text{-}[xant(P^iPr_2)_2]\}$ (**6**) with HBcat leads to the σ-borane derivative $OsH_2(\eta^2\text{-}H\text{-}Bcat)\{\kappa^3\text{-}P,O,P\text{-}[xant(P^iPr_2)_2]\}$ (**7**), which shows a distance between the atoms of the coordinated B-H bond in the range 1.4-1.5 Å. AIM analysis for the OsHB unit of **7** only displays Os-B and B-H bond critical points therefore lacking a similar topology.

INTRODUCTION

Metal-promoted σ-bond activation reactions are the origin of a great number of processes in the current chemistry. The first step is the coordination of the σ-bond to the metal to form a σ-complex. The metal-bond interaction involves σ-donation from the σ-molecular orbital of the coordinated bond to empty orbitals of the metal and back bonding from the metal to the σ*-molecular orbital of the bond. The balance between donation and back-donation determines the degree of addition of the bond to the metal, which in the majority of cases fits to the separation between the coordinated atoms.[1] Dihydrogen compounds form the best-known group of complexes of this type. Depending upon the separation between the coordinated hydrogens, they are classified in Kubas-type complexes (0.8-1.0 Å) and elongated dihydrogens (1.0-1.3 Å). High oxidation states, first-row metals, cationic charges, acidic ligands and tridentate groups enforcing L-M-L angles close to 90º stabilize Kubas-type complexes while low oxidation states, third-row metals, and π-donor ligands favor the formation of elongated dihydrogen compounds.[2]

The stabilization of σ-E-H bond activation intermediates (B, C, Si, etc) is much more difficult than the stabilization of dihydrogen species.[3] As a consequence, very little information is available for σ-E-H complexes. By comparison to the hydrogen molecule, an R_nE-H bond (n = 2 or 3) is dissymmetric and the substituents at the E atom may tune the acidity of the bond. In addition, in some cases the E atom can possess available empty orbitals, as boron, which alter the balance between donation and back-donation in comparison with the dihydrogen situation.

The B-H bond activation is a reaction of great interest in connection with the borylation of organic molecules[4] and the dehydrocoupling of amineboranes.[5] However, scarce examples of complexes containing non-assisted B-H coordination have been reported.[6] They include some first-row metals; such as Ti,[7] Mn, Re,[8] Ni;[9] and Ru.[10] These compounds contain small H-M-B angles (32º-38º), whereas the B-H distances are in the range 1.23-1.35 Å. For third-row metals, Heinekey and coworkers have reported the neutron diffraction structure of $IrH_2\{\kappa^3\text{-}P,C,P\text{-}[C_6H_3\text{-}1,3\text{-}(OP^tBu_2)_2]\}(\eta^2\text{-}H\text{-}BH_2)$, which contains a B-H σ-bond coordinated to iridium with a B-H distance of 1.45(5) Å. The pinacolborane (HBpin) counterpart losses molecular hydrogen to afford the square planar derivative $Ir\{\kappa^3\text{-}P,C,P\text{-}[C_6H_3\text{-}1,3\text{-}(OP^tBu_2)_2]\}(\eta^2\text{-}H\text{-}Bpin)$.[11] Our group has described the coordination of catecholborane (HBcat) and HBpin to the osmium dihydride $OsH_2(CO)(P^iPr_3)_2$ to give $OsH_2(CO)(\eta^2\text{-}H\text{-}BR_2)(P^iPr_3)_2$.[12] There are also a few (C_5Me_5)Rh-complexes bearing hydride and boryl ligands, which show separations between the boron and a hydride in the range 1.60-2.0 Å.[13] For these compounds, which could be considered the borane counterparts of the elongated dihydrogen species on the base of this separation, a "residual" B···H interaction has been suggested, although no clear evidence on

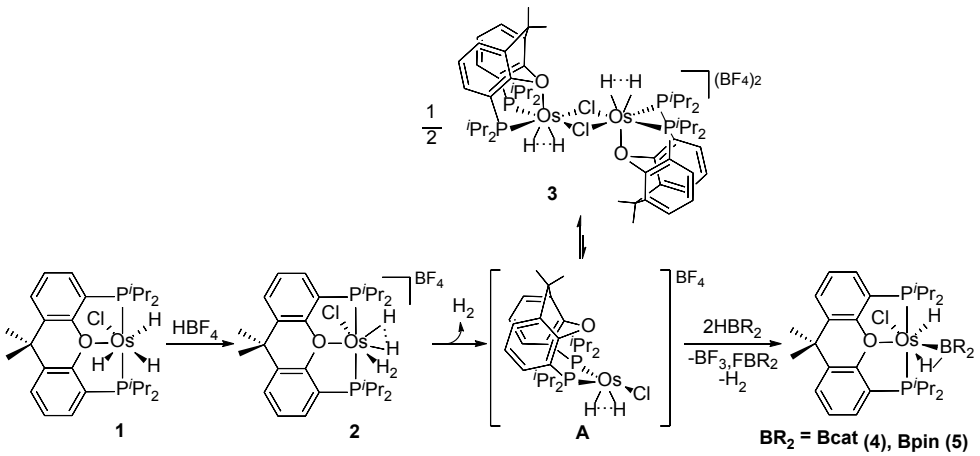

Scheme 1. Formation of Elongated σ-Borane complexes **4** and **5.**

their nature has been provided. In contrast to dihydrogen complexes, it remains difficult to assign a correct formulation on the basis of ^{11}B and ^{1}H NMR.[14] Thus, the development of simple methods to assert nature of the interaction of the B-H bond with the metal center, discerning between σ-borane and elongated σ-borane, is a need of the field.

Ether-diphosphines (POP) are flexible, which allows them to change their coordination fashion for adapting to the requirement of the participating intermediates in multistep processes.[15] As a consequence of this ability, platinum group metals containing these ligands are playing a main role in homogeneous catalysis.[16] In addition, we have recently shown that osmium polyhydrides bearing 9,9-dimethyl-4,5-bis(diisopropylphosphine)xanthene (xant(P^iPr_2)$_2$) sequentially add H^+ and H^- or H^- and H^+ to generate molecular hydrogen in a cyclic manner. During the process the ether-diphosphine changes its coordination mode to stabilize both dihydride and dihydrogen species. Dihydrogens are favored by a *mer* disposition of its donor atoms.[17] The ability of the *mer*-Os(POP) skeleton to stabilize non-classical interactions prompted us to study the coordination of HBcat and HBpin to OsHX(POP) metal fragments (X=H, Cl), in order to analyze the influence of the X ligand on the addition degree of the B-H bond to the osmium atom.

This paper describes the formation of new elongated σ-borane and σ-borane complexes for a third-row metal of the platinum group; shows the first X-ray structures for this type of compounds in the osmium chemistry; and analyzes the osmium-borane bonding situation as a function of X, proving that Atom in Molecules (AIM), Natural Bond Orbital (NBO), and Energy Decomposition Analysis-Natural Orbital for Chemical Valence (EDA-NOCV) methods are a simple tool to distinguish between σ-borane and elongated σ-borane.

RESULTS AND DISCUSSION

Elongated σ-Boranes. We have recently shown that the trihydride derivative $OsH_3Cl\{\kappa^3$-*P*,*O*,*P*-[xant(P^iPr_2)$_2$]} (**1**) adds the proton of HBF_4 to afford the compressed dihydride-dihydrogen cation $[Os(H\cdots H)(\eta^2$-$H_2)Cl\{\kappa^3$-*P*,*O*,*P*-[xant(P^iPr_2)$_2$]}]$^+$ (**2**), which is stable under hydrogen atmosphere. Under argon, it dissociates the coordinated hydrogen molecule and the resulting unsaturated dihydride $[OsH_2Cl\{\kappa^2$-*P*,*P*-[xant(P^iPr_2)$_2$]}]$^+$ (**A**) rapidly reaches an equilibrium with the dimer $[(Os(H\cdots H)\{\kappa^3$-*P*,*O*,*P*-[xant($P^iPr_2$)$_2$]})$_2(\mu$-$Cl)_2]^{2+}$ (**3**). During the dimerization process, the ether-diphosphine changes its coordination fashion from κ^3-*mer* to κ^3-*fac*.[17] Now, we have observed that HBcat and HBpin trap the unsaturated dihydride **A**. In addition, the metal center promotes the heterolytic H-B bond activation of a borane molecule by using a fluoride of the $[BF_4]^-$ anion as an external base. Thus, the treatment of dichloromethane solutions of the BF_4-salt of **3** with 5.1 mol of HBcat and HBpin, at room temperature, for 10 min leads to the hydride-elongated σ-borane derivatives $OsHCl(\eta^2$-H-$BR_2)\{\kappa^3$-*P*,*O*,*P*-[xant(P^iPr_2)$_2$]}(BR_2 = Bcat (**4**), Bpin (**5**)), which were isolated as white solids in 50-60% yield, together with FBR_2 ($\delta_{11B,}$ 22.5), BF_3 (δ_{11B}, 0.0), and H_2 (Scheme 1).

Complex **4** was characterized by X-ray diffraction analysis. The structure has two molecules chemically equivalent but crystallographically independent in the asymmetric unit. Figure 1 shows a view of one of them. The ether-diphosphine is *mer* coordinated with P(1)-Os-P(2), P(1)-Os-O(3), and P(2)-Os-O(3) angles of 161.98(3)° and 161.85(3)°, 80.98(6)° and 81.30(6), and 81.27(6) and 80.90(6), respectively. Thus, the coordination polyhedron around the metal center can be rationalized as a distorted octahedron. The perpendicular plane to the P(1)-Os-P(2) direction contains the hydride H(01) ligand disposed trans to the oxygen atom of the ether-diphosphine (H(01)-Os-O(3) = 165.6(9)° and 166.2(9)°) and the coordinated catecholborane molecule situated trans to the chloride ligand with the hydrogen atom H(02) pointing out the ether. The coordination of the B-H bond promotes its elongation. The B-H(02) distances of 1.68(2) and 1.67(2) Å, 1.601 Å in the DFT-optimized structure, agree well with the shortest B-H distance in the rhodium complex $Rh(\eta^5$-$C_5Me_5)(Bpin)_2(\eta^2$-HBpin) (1.53(3) and 1.69(3) Å)[13] and support the elongated σ-borane character of this species. The B-M-H angles in both compounds are also similar, 53.6(9)° and 53.1(9)° in **4** *versus* 47.5(8)° and 54.3(10)° in the rhodium derivative. The B-H(02) distance is about 0.5 Å longer than the B-H(Os) bond lengths in the tetrahydridoborate derivative $OsH_3(\kappa^2$-$H_2BH_2)$(IPr)(P^iPr_3) (1.18(3) and 1.17(3) Å. IPr = 1,3-bis(2,6-diisopropylphenylimidazolylidene)[18] and about 0.4 Å longer than the B-H(Os) distances in the dihydrideborate species Os(Bcat)(κ^2-H_2Bcat)(CO)(P^iPr_3) (1.26(3) and 1.27(3) Å).[12b] However, interestingly, the B-H(02) distance is only slightly shorter than the separation between the boron atom and the hydride ligand H(01), 1.70(2) and 1.70(2) Å; 1.770 Å in the

DFT-optimized structure. This is consistent with a *cis*-hydride-elongated σ-borane interaction. "Residual" contacts of this type are common in *cis*-hydride-elongated dihydrogen species.[2c,19] Nevertheless, in this case, it does not appear to involve a true covalent bond (*vide infra*). It seems to be related to the geometry of the complex and the size of the involved atoms and could be magnified by the different sign of the partial charges on the hydride and on the boron atom of the borane. The interaction between the metal center and the coordinated B-H bond is certainly strong. Thus, the Os-B bond lengths of 2.036(4) and 2.042(4) Å, 2.054 Å in the DFT-optimized structure, compare well with the reported Os-boryl distances.[12,20]

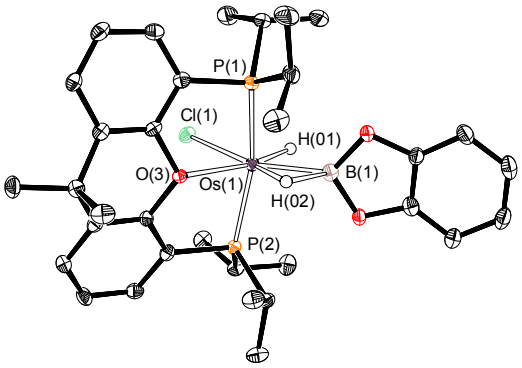

Figure 1. ORTEP diagram of one of the two molecules chemically equivalent but crystallographically independent in the asymmetric unit of the complex **4** with 50 % probability ellipsoids. The solvent molecule and hydrogen atoms (except H(01) and H(02)) are omitted for clarity. Selected bond lengths (Å) and angles (deg): Os(1)-B(1) = 2.036(4) and 2.042(4), Os(1)-O(3) = 2.259(2) and 2.251(2), Os(1)-P(2) = 2.3047(8) and 2.3175(8), Os(1)-P(1) = 2.3167(8) and 2.3046(8), Os(1)-Cl(1) = 2.4694(8) and 2.4694(8), Os(1)-H(01) = 1.582(10) and 1.588(10), Os(1)-H(02) = 1.590(10) and 1.585(10), B(1)-H(01) = 1.70(2) and 1.70(2), B(1)-H(02) = 1.68(2) and 1.67(2), P(1)-Os(1)-P(2) = 161.98(3) and 161.85(3), P(2)-Os(1)-O(3) = 81.27(6) and 80.90(6), P(1)-Os(1)-O(3) = 80.98(6) and 81.30(6), B(1)-Os(1)-H(02) = 53.6(9) and 53.1(9), O(3)-Os(1)-H(01) = 165.6(9) and 166.2(9).

Complex **5** was also characterized by X-ray diffraction analysis. Figure 2 shows a view of the molecule. The coordination polyhedron around the osmium atom resembles that of **4** with a H-Bpin group instead of the H-Bcat ligand and P-Os-P, P-Os-O(2), and H(01)-Os-O(2) angles of 163.05(2)°, 81.577(11)°, and 165.9(10)°, respectively. The strength of the interaction between the B-H bond and the metal center is similar in both compounds. Thus, the B-H(02) and Os-B distances of 1.69(2) and 2.075(3) Å, respectively, 1.623 and 2.071 Å in the DFT-optimized structure, compare well with those of **4**.

The $^{31}P\{^{1}H\}$, ^{1}H, and ^{11}B NMR spectra of **4** and **5** are consistent with the structures depicted in Figures 1 and 2. In agreement with the *mer*-coordination of the ether-diphosphine, the $^{31}P\{^{1}H\}$ NMR spectra, in benzene-d_6, at room temperature contain a singlet at about 36 ppm. Under the same conditions, the hydride ligand of **4** gives rise to a broad signal at -11.44 ppm in the ^{1}H NMR spectrum, which splits into a triplet ($^{2}J_{H\text{-}P}$ = 11.0 Hz) in dichloromethane-d_2 at 243 K, whereas the hydride ligand of **5** displays a triplet ($^{2}J_{H\text{-}P}$ = 11.0 Hz) at -12.99 ppm. In contrast to the hydride ligand, the coordinated BH-hydrogen atom gives rise to a broad resonance at -16.59 ppm for **4** and -16.99 ppm for **5**, at 243 K and at room temperature. The ^{11}B NMR spectra, in benzene-d_6, at room temperature shows a broad signal at 52.0 ppm for **4** and 46.5 pm for **5**.

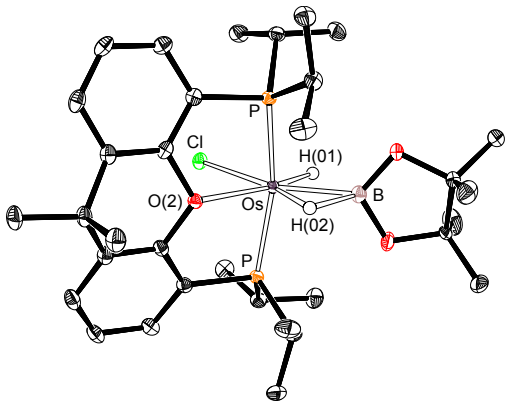

Figure 2. ORTEP diagram of complex **5** with 50 % probability ellipsoids. Hydrogen atoms (except H(01) and H(02)) are omitted for clarity. Selected bond lengths (Å) and angles (deg): Os-B(1) = 2.075(3), Os-O(2) = 2.2644(15), Os-P = 2.2989(4), Os-Cl = 2.4603(5), Os-H(01) = 1.577(10), Os-H(02) = 1.586(10), B(1)-H(01) = 1.75(3), B(1)-H(02) = 1.69(2), P-Os-P = 163.05(2), P-Os-O(2) = 81.577(11), H(01)-Os-O(2) = 165.9(10), B(1)-Os-H(02) = 53.1(9).

σ-Borane. In spite of its thermal stability and low tendency to undergo reductive elimination of molecular hydrogen,[21] the classical tetrahydride $OsH_4\{\kappa^3\text{-}P,O,P\text{-}[xant(P^iPr_2)_2]\}$ (**6**) rapidly reacts with HBcat. The addition of 1.1 mol of the borane to benzene solutions of **6** leads to the osmium(II)-dihydride-σ-borane derivative $OsH_2(\eta^2\text{-H-Bcat})\{\kappa^3\text{-}P,O,P\text{-}[xant(P^iPr_2)_2]\}$ (**7**), as a result of the formal replacement of a hydrogen molecule by the B-H bond of HBcat (eq. 1).

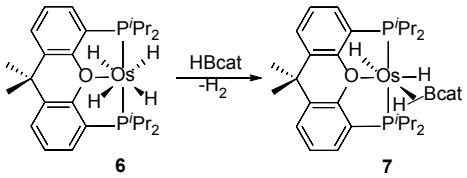

(1)

Complex **7** was isolated as a white solid in 80% yield and characterized by X-ray diffraction analysis. Figure 3 shows a view of the molecule. The ether-diphosphine is *mer*-coordinated with P(1)-Os-P(2), P(1)-Os-O(3), and P(2)-Os-O(3) angles of 161.89(4)°, 82.06(7)°, and 81.29(7)°, respectively. Thus, the coordination polyhedron around the metal center is similar to that found for **4** with a hydride ligand (H(03)) in the position of the chloride anion and a H(02)-Os-O(3) angle of 162.6(17)°. The chloride by hydride replacement decreases the strength of the interaction between the metal center and the borane. As a consequence, the B-H distance of 1.49(4) Å (B(1)-H(01)), 1.434 Å in the DFT-optimized structure, is between 0.1 and 0.2 Å shorter than in **4**. The B-Os-H angle of 45.5(15)° (B(1)-Os-H(01)) is also smaller. Both the B-H distance and the B-M-H angle are similar to those reported for the iridium complex $Ir\{\kappa^3\text{-}P,C,P\text{-}[C_6H_3\text{-}1,3\text{-}(OP^tBu_2)_2]\}(\eta^2\text{-H-Bpin})$ (1.47(6) Å and 45(2)°).[11] As expected, and in contrast to the B-H bond length, the Os-B distance of 2.057(4) Å, 2.088 Å in the DFT-optimized structure, is between 0.02 and 0.04 Å longer than in **4**. Like in the later, the boron atom and its *cisoid* hydride H(02) are close, although

the separation between them of 1.81(4) Å, 1.926 Å in the DFT-optimized structure, is about 0.1-0.2 Å longer than in **4**; i.e., the boron atom moves away from the hydride the same as approaches the hydrogen atom. This again suggests that in these compounds the proximity between the boron atom and the hydride is a consequence of the geometry of the complexes and the size of the involved atoms.

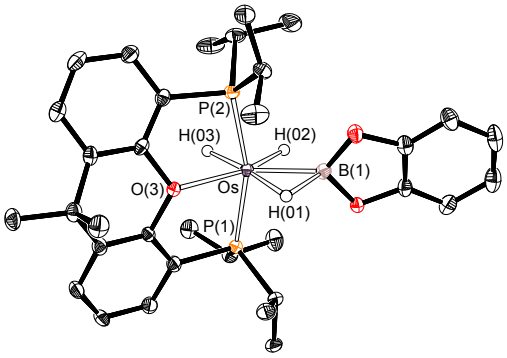

Figure 3. ORTEP diagram of complex **7** with 50 % probability ellipsoids. Hydrogen atoms (except H(01), H(02) and H(03)) are omitted for clarity. Selected bond lengths (Å) and angles (deg): Os-B(1) = 2.057(4), Os-O(3) = 2.271(3), Os-P(1) = 2.2832(10), Os-P(2) = 2.2808(10), Os-H(01) = 1.69(5), Os-H(02) = 1.579(14), Os-H(03) = 1.590(14), B(1)-H(01) = 1.49(4), B(1)-H(02) = 1.81(4), P(1)-Os-P(2) = 161.89(4), P(1)-Os-O(3) = 82.06(7), P(2)-Os-O(3) = 81.29(7), H(02)-Os-O(3) = 162.6(17), B(1)-Os-H(01) = 45.5(15).

The ^{1}H, ^{11}B, and ^{31}P{^{1}H} NMR spectra of **7** are consistent with the structure shown in the Figure 3. The ^{1}H NMR spectrum, in toluene-d_8, at 193 K shows the B-H resonance at -1.9 ppm along with the signals corresponding to the inequivalent hydrides at -5.60 and -18.8 ppm. The B-H resonance is temperature invariant between 193 and 298 K. However, the hydride signals are temperature dependent (Figure 4). Thus, they coalesce at 233 K and a hydride signal is observed above this temperature. Figure 4 reveals that the hydride ligands undergo a thermally activated site exchange process, which takes place with an activation barrier of 9 kcal·mol^{-1}.[22] This behavior agrees well with that observed for the iridium complex $IrH_2\{\kappa^3$-*P*,*C*,*P*-[C_6H_3-1,3-(OP^tBu_2)$_2$]}(η^2-HBpin)[11] and the osmium-carbonyl derivatives $OsH_2(CO)(\eta^2$-H-$BR_2)(P^iPr_3)_2$ (BR_2 = Bcat, Bpin).[12] The presence of the coordinated H-B bond is also supported by the ^{11}B NMR spectrum at room temperature, which contains a broad resonance centered at 45.5 ppm. A singlet at 56.0 ppm in the ^{31}P{^{1}H} NMR spectrum is another characteristic feature of this complex.

The promptly formation of **7** according to eq 1 is not consistent with the saturated character of **6** neither with a dissociation of the xanthene-ether group prior to the borane coordination. Because transition metal hydride complexes are usually amphoteric,[23] they can experience autoionization. In the case of **7**, this should imply the formation of the previously described pentahydride $[OsH_5\{\kappa^2$-*P*,*P*-[xant(P^iPr_2)$_2$]}]$^-$ (**8**),[17] containing a *P*,*P*-bidentate ether-diphosphine, and the unsaturated osmium (IV) cation $[OsH_3\{\kappa^3$-*P*,*O*,*P*-[xant(P^iPr_2)$_2$]}]$^+$ (**B** in eq 2). Thus, the boron atom of the borane could undergo the nucleophilic attack of the pentahydride, which should give rise to the release of a hydride and the formation of OsH_5(Bcat)$\{\kappa^2$-*P*,*P*-[xant(P^iPr_2)$_2$]} (**C**), a boryl-pentahydride counterpart of the previously reported hexahydride $OsH_6\{\kappa^2$-

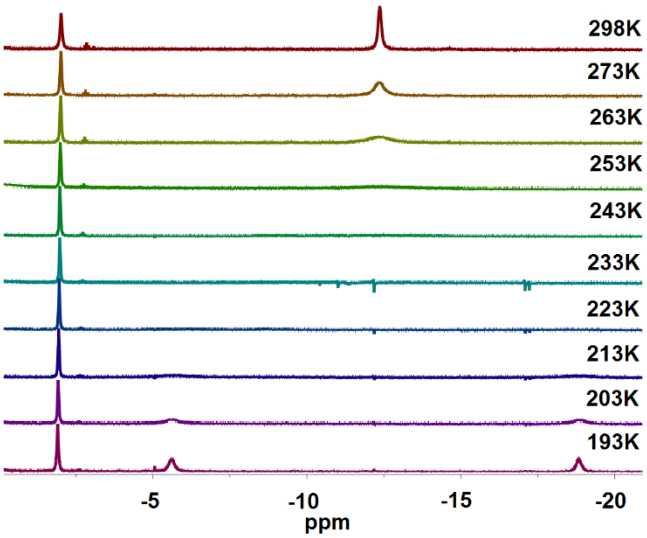

Figure 4. High-field region of the ^{1}H NMR spectrum of **7** between 298 and 193 K.

P,*P*-[xant(P^iPr_2)$_2$]}[16d] (eq 3). Then, the generated hydride should be trapped by the cation **B** to again afford **6** (eq 4), which could further react in the same way until the consumption of the borane, whereas the coordination of the oxygen atom of the xanthene group of **C** should produce the release of molecular hydrogen and the formation of **7** (eq 5).

$$2\ OsH_4\{\kappa^3\text{-}P,O,P\text{-}[xant(P^iPr_2)_2]\} \rightleftharpoons$$
6

$$\rightleftharpoons [OsH_5\{\kappa^2\text{-}P,P\text{-}[xant(P^iPr_2)_2]\}]^- + [OsH_3\{\kappa^3\text{-}P,O,P\text{-}[xant(P^iPr_2)_2]\}]^+ \quad (2)$$
8 **B**

$$[OsH_5\{\kappa^2\text{-}P,P\text{-}[xant(P^iPr_2)_2]\}]^- + HBcat \longrightarrow$$
8

$$\longrightarrow OsH_5(Bcat)\{\kappa^2\text{-}P,P\text{-}[xant(P^iPr_2)_2]\} + H^- \quad (3)$$
C

$$[OsH_3\{\kappa^3\text{-}P,O,P\text{-}[xant(P^iPr_2)_2]\}]^+ + H^- \longrightarrow$$
B

$$\longrightarrow OsH_4\{\kappa^3\text{-}P,O,P\text{-}[xant(P^iPr_2)_2]\} \quad (4)$$
6

$$OsH_5(Bcat)\{\kappa^2\text{-}P,P\text{-}[xant(P^iPr_2)_2]\} \longrightarrow$$
C

$$\longrightarrow OsH_2(\eta^2\text{-H-Bcat})\{\kappa^3\text{-}P,O,P\text{-}[xant(P^iPr_2)_2]\} + H_2 \quad (5)$$
7

The formation of **7** according to the 2-5 reactions sequence involves the heterolytic addition of the H-B bond of HBcat to different metal centers. In order to prove that this reactions sequence is a reasonable proposal, we carried out the reaction of **6** with ClBcat. As expected, the addition of 0.5 equiv of the boron reagent to a benzene-d_6 solution of the tetrahydride immediately gives a quantitative 1:1 mixture of **7** and **1** (eq 6).

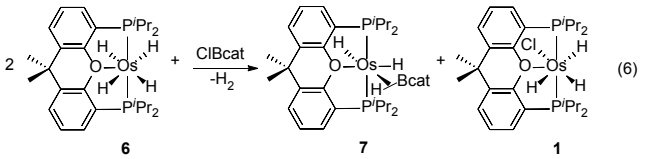

(6)

Bonding Situation. The bonding situation in complexes **4** and **7** was analyzed by means of DFT calculations, using the dispersion corrected BP86-D3 functional. The nature of the osmium-boron interactions was investigated using AIM, NBO, and EDA-NOCV methods. Figure 5 shows the Laplacian

distributions in the Os−H−B plane for complexes **4** and **7**. Both species exhibit a significant Os−B interaction as revealed by the occurrence of a bond critical point (BCP) located between the transition metal and the boron atom, which is associated with a bond path (BP) running between both atoms. Interestingly, whereas a BCP between the osmium and the adjacent hydrogen atom close to the boron is located in complex **4**, no such Os−H interaction is found for complex **7** (i.e. absence of a BCP and corresponding BP between both atoms). This finding is consistent with the calculated Wiberg Bond Indices (WBI) for the respective Os–B and Os–H bonds. Thus, whereas similar WBIs were computed for the Os–B bond of both complexes (WBI = 0.68 and 0.65, for compounds **4** and **7**, respectively), rather different indices were computed for the Os–H interaction. Indeed, the much lower WBI value of 0.36 computed for **7** (WBI = 0.51 for **4**) clearly suggests that the Os–H interaction is much weaker in **7** than in **4**. As a consequence, no BCP was located in the corresponding AIM diagram. Therefore, the NBO and AIM methods indicate that although the Os–B bond strength is rather similar in both complexes, their bonding situations are markedly different. While the elongated σ-borane complex **4** is characterized by a three-membered cyclic species possessing one OsBH ring critical point, the σ-borane compound **7** lacks this triangular topology.

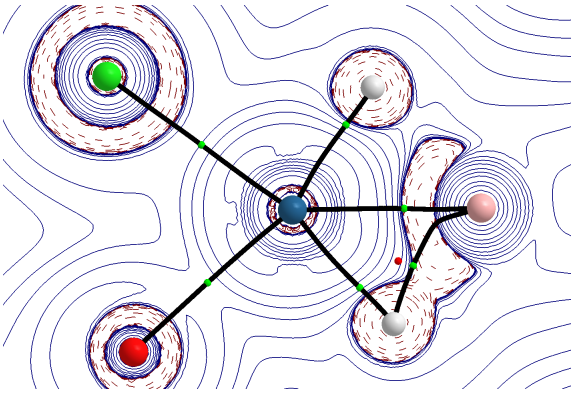

4

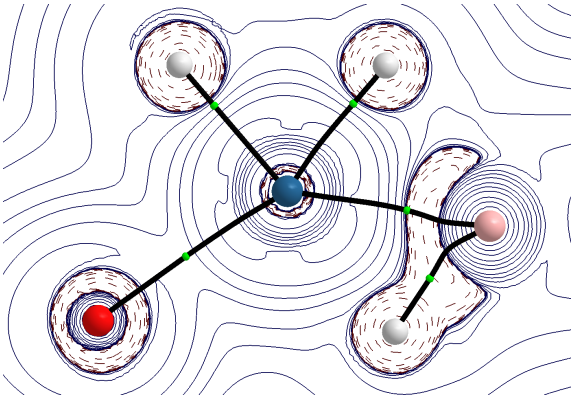

7

Figure 5. Contour line diagrams $\nabla^2\rho(r)$ for complexes **4** and **7** in the O−Os−B plane. Solid lines indicate areas of charge concentration ($\nabla^2\rho(r) < 0$) while dashed lines show areas of charge depletion ($\nabla^2\rho(r) > 0$). The solid lines connecting the atomic nuclei are the bond paths while the small green and red spheres indicate the corresponding bond critical points and ring critical points, respectively. H (●); O (●); Cl (●); Os (●); B(●).

In order to gain more quantitative insight into the bonding situation of complexes **4** and **7**, the EDA-NOCV method was applied next. This method combines charge (NOCV) and energy (EDA) partitioning schemes to decompose the deformation density which is associated with the bond formation, Δρ, into different components of the chemical bond. The EDA-NOCV calculations provide pairwise energy contributions for each pair or interacting orbitals to the total bond energy (see further details in the computational details section).

The interaction between the neutral, closed-shell fragments OsHX(POP) and HBcat (X = Cl(**4**), H(**7**)) was considered for both complexes **4** and **7**. From the data in Table 1, it becomes evident that the above discussed weaker Os–H interaction in the σ-borane complex **7** leads to a significant reduction of the interaction between the HBcat ligand and the transition metal moiety with respect to complex **4** ($\Delta\Delta E_{int}$ = 31.9 kcal/mol). The EDA suggests that, despite the lower Pauli repulsion, this reduced interaction in complex **7** is mainly due to less stabilizing electrostatic ($\Delta\Delta E_{elstat}$ = 59.3 kcal/mol) and orbital ($\Delta\Delta E_{orb}$ = 34.7 kcal/mol) attractions.

Table 1. EDA-NOCV results (in kcal/mol) computed at the ZORA-BP86-D3/TZ2P+//BP86-D3/def2-SVP level.

	4	**7**
ΔE_{int}	-118.2	-86.3
ΔE_{Pauli}	298.3	234.7
ΔE_{elstat} [a]	-244.1 (58.6%)	-184.8 (57.6%)
ΔE_{orb} [a]	-160.8 (38.6%)	-126.1 (39.3%)
$\Delta E(\rho_1)$ [b]	-47.2 (29.3%)	-28.9 (22.9%)
$\Delta E(\rho_2)$ [b]	-83.9 (52.2%)	-71.6 (56.8%)
ΔE_{rest} [b]	-29.7 (18.5%)	-25.6 (20.3%)
ΔE_{disp} [a]	-11.5 (2.8%)	-10.1 (3.1%)

[a] Values within parentheses indicate the percentage to the total interaction energy, $\Delta E_{int} = \Delta E_{Pauli} + \Delta E_{elstat} + \Delta E_{orb} + \Delta E_{disp}$. [b] Values in parentheses are the percentage contributions to the total orbital interactions ΔE_{orb}.

The NOCV method provides further quantitative insight into the contributions to the total orbital attractions, which illustrate the different bonding situations in these complexes. Figure 6 shows the computed deformation densities Δρ, which indicate the charge flow in these species (the charge flow takes place in the direction red→blue). From the data in Figure 6, two main orbital interactions describe the σ-borane bonding situation, namely the donor-acceptor interaction involving the doubly-occupied σ(B–H) molecular orbital and a vacant d atomic orbital of the transition metal (ρ_1) and the reverse d(Os)→σ*(B–H) back-donation (ρ_2). According to the computed associated energies, both orbital interactions are significantly stronger in complex **4**, which is translated into the computed higher total orbital interactions (ΔE_{orb}) for this complex (see Table 1). Not surprisingly, the donation from the σ(B–H) molecular orbital is significantly stronger in complex **4** ($\Delta\Delta E(\rho_1)$ = 18.3 kcal/mol) due to the much higher electron withdrawing ability of the chloride ligand as compared to the hydride ligand in complex **7**. As a consequence of this stronger donation and the higher population of the corresponding σ*(B–H) molecular orbital ($\Delta\Delta E(\rho_2)$ = 12.3 kcal/mol), the B–H bond is significantly longer in complex **4** (1.601 Å, exp.

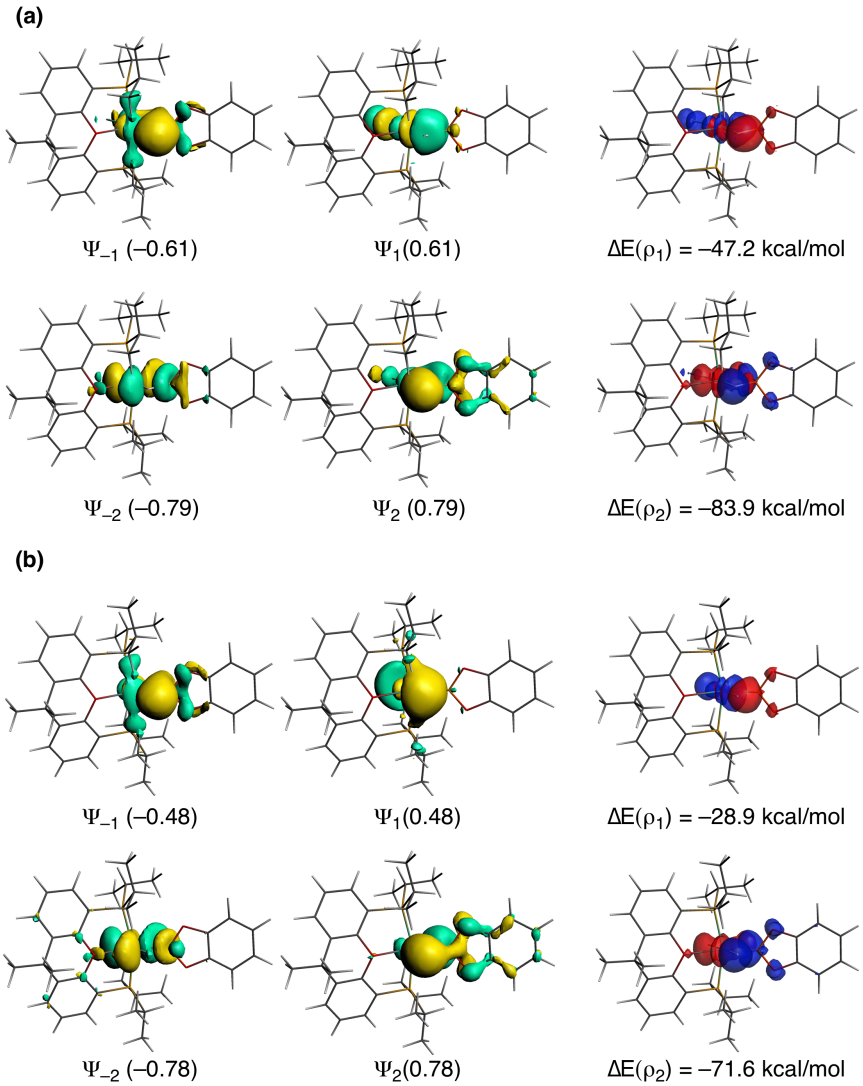

Figure 6. Most important NOCV pairs of orbitals Ψ_{-k}, Ψ_k with their eigenvalues $-\upsilon_k$, υ_k given in parentheses, and the associated deformation densities $\Delta\rho_k$ and orbital stabilization energies ΔE for the complexes **4** (a) and **7** (b). The charge flow in the deformation densities takes place in the direction red to blue.

1.68(2) and 1.67(2) Å) than in complex **7** (1.434 Å, exp. 1.49(4) Å). A similar effect has been observed for the coordination of dimethylaminoborane to the ruthenium fragments $RuHX(P^iPr_3)_2$ (X = H, Cl).[24]

CONCLUDING REMARKS

This study has revealed that the square pyramidal metal fragments $OsHX\{\kappa^3\text{-}P,O,P\text{-}[xant(P^iPr_2)_2]\}$ (X = Cl, H) stabilize the coordination of the B-H bond of boranes *trans* to the X ligand. The strength of the interaction between the metal center and the borane, which involves σ-donation from the doubly occupied σ(B-H) orbital to a vacant d atomic orbital of the metal and d(Os)→σ*(B-H) back-donation, is sensitive to the nature of X, being favored for chloride with regard to hydride. The electron withdrawing ability of the chloride ligand increases the donation from the σ(B-H) orbital to the osmium atom, whereas its π-donor power favors the d(Os)→σ*(B-H) back-donation. As a result, the coordinated B-H bond is significantly longer for complex **4** (X = Cl) than for **7** (X = H). The EDA-NOCV analysis suggests that the computed much lower interaction strength between the metal fragment $OsH_2\{\kappa^3\text{-}P,O,P\text{-}[xant(P^iPr_2)_2]\}$ and the borane is mainly due to less stabilizing electrostatic and orbital attractions.

The coordination of the borane to the metal fragment $OsHCl\{\kappa^3\text{-}P,O,P\text{-}[xant(P^iPr_2)_2]\}$ affords elongated σ-borane species, whereas the coordination to the dihydride counterpart $OsH_2\{\kappa^3\text{-}P,O,P\text{-}[xant(P^iPr_2)_2]\}$ gives a σ-borane compound. NBO-AIM analysis shows marked differences in the bonding situation of both types of derivatives. While elongated σ-borane complexes are characterized by a three-membered cycle possessing one OsBH ring critical point, the σ-borane compound lacks this triangular topology.

In conclusion, related elongated σ-borane and σ-borane complexes stabilized by OsHX(POP) metal fragments have been isolated, fully characterized, and the interaction between the metal fragments and the coordinated B-H analyzed as a function of X, from spectroscopic, X-ray diffraction, and theoretical points of view.

EXPERIMENTAL SECTION

General Information. All reactions were carried out under argon with rigorous exclusion of air using Schlenk tube or glovebox tech-

niques. Solvents were dried by the usual procedures and distilled under argon prior to use or obtained oxygen- and water-free from an MBraun solvent purification apparatus. Pentane and dichloromethane were further stored over P_2O_5 in the glovebox. Toluene and benzene were stored over sodium in the glovebox. Pinacolborane was purchased from commercial sources and used without further purification. Catecholborane was purchased from commercial sources and distilled in a Kugelrohr distillation oven. Complexes $OsH_3Cl\{\kappa^3$-*P*,*O*,*P*-[xant(P^{i}Pr$_2$)$_2$]} (**1**),[16d] [(Os(H···H)$\{\kappa^3$-*P*,*O*,*P*-[xant(P^{i}Pr$_2$)$_2$]$\}_2(\mu$-Cl)$_2][BF_4]_2$ (**3**),[17] and $OsH_4\{\kappa^3$-*P*,*O*,*P*-[xant(P^{i}Pr$_2$)$_2$]} (**6**),[16d] were prepared according to published methods. ^{1}H, ^{31}P$\{^1$H$\}$, ^{11}B and ^{13}C$\{^1$H$\}$ NMR spectra were recorded on either a Bruker 300 ARX, Bruker Avance 300 MHz or a Bruker Avance 400 MHz instrument. Chemical shifts (expressed in parts per million) are referenced to residual solvent peaks (^{1}H, ^{13}C$\{^1$H$\}$) or external H_3PO_4 (^{31}P$\{^1$H$\}$) and $BF_3{\cdot}OEt_2$ (^{11}B). Coupling constants, *J* and *N* ($N = J_{PH} + J_{P'H}$ for ^{1}H; $N = J_{PC} + J_{P'C}$ for ^{13}C) are given in hertz. Spectral assignments were achieved by ^{1}H-^{1}H COSY, ^{1}H$\{^{31}$P$\}$, ^{13}C APT, ^{1}H-^{13}C HSQC and ^{1}H-^{13}C HMBC experiments. C and H analyses were carried out in a Perkin-Elmer 2400 CHNS/O analyzer. High-resolution electrospray mass spectra were acquired using a Micro-TOF-Q hybrid quadrupole time-of-flight spectrometer (Bruker Daltonics, Bremen, Germany).

Synthesis of OsHCl(η^2-H-Bcat)$\{\kappa^3$-*P*,*O*,*P*-[xant(P^{i}Pr$_2$)$_2$]} (4). To a suspension of [(Os(H···H)$\{\kappa^3$-*P*,*O*,*P*-[xant(P^{i}Pr$_2$)$_2$]$\}_2(\mu$-Cl)$_2][BF_4]_2$ (**3**) (50 mg; 0.033 mmol) in CH_2Cl_2 (3 mL) was added HBcat (18 µl; 0.169 mmol). After 10 min, the colorless solution obtained was taken to dryness. Addition of pentane (1mL) to the residue allowed the precipitation of a white solid, which was washed twice with pentane (2 mL) and dried under vacuum. Yield: 29 mg (56 %). Colorless crystals suitable for X-ray diffraction analysis were obtained by vapor diffusion of pentane into a toluene solution of the complex. Anal. Calcd. for $C_{33}H_{46}BClO_3OsP_2$: C, 50.23; H, 5.88. Found: C, 50.03; H, 5.95. HRMS (electrospray, m/z): calcd. for $C_{33}H_{46}BClNaO_3OsP_2$ $[M + Na]^+$: 813.2207, found: 831.2185. HRMS (electrospray, m/z): calcd. for $C_{33}H_{46}BO_3OsP_2$ $[M-Cl]^+$: 755.2632, found: 755.2600. ^{1}H NMR (300.13 MHz, C_6D_6, 293K): δ 7.32 (m, 2H, C*H*-arom), 7.16 (m, 2H, C*H*-arom), 7.15 (m, 2H, C*H*-arom Bcat), 7.03 (dd, $^3J_{HH}$ = 7.6, $^3J_{HH}$ = 7.5, 2H, C*H*-arom), 6.92 (m, 2H, C*H*-arom Bcat), 3.12 (m, 2H, PC*H*(CH$_3$)$_2$), 3.00 (m, 2H, PC*H*(CH$_3$)$_2$), 1.83 (dvt, $^3J_{HH}$ = 7.1, *N* = 14.5, 6H, PCH(C*H*$_3$)$_2$), 1.74 (dvt, $^3J_{HH}$ = 7.5, *N* = 16.1, 6H, PCH(C*H*$_3$)$_2$), 1.45 (s, 3H, C*H*$_3$), 1.11 (s, 3H, C*H*$_3$), 1.23-0.92 (12H, PCH(C*H*$_3$)$_2$), -11.44 (br, 1H, Os*H*), -15.73 (br, 1H, Os*H*). ^{1}H NMR (400.13 MHz, CD_2Cl_2, 243K): δ -12.53 (t, 1H, $^2J_{HP}$ = 11.0, Os*H*), -16.59 (br, 1H, Os(η^2-*H*-Bcat)). ^{13}C$\{^1$H$\}$-APT NMR (75.47 MHz, C_6D_6, 293K): δ 158.9 (vt, *N* = 12.5, *C*-arom), 152.5 (s, *C* Bcat), 132.6 (vt, *N* = 5.6, *C*-arom), 130.8 (s, *C*H-arom), 126.9 (s, *C*H-arom), 126.3 (vt, *N* = 27.9, *C*-arom), 124.9 (vt, *N* = 4.8, *C*H-arom), 120.6 (s, *C*H-arom Bcat), 110.2 (s, *C*H-arom Bcat), 35.1 (s, C(*C*H$_3$)$_2$), 34.2 (s, *C*(CH$_3$)$_2$), 28.0 (vt, *N* = 29.6, P*C*H(CH$_3$)$_2$), 25.3 (vt, *N* = 25.5, P*C*H(CH$_3$)$_2$), 24.5 (s, C(*C*H$_3$)$_2$), 21.0 (s, PCH(*C*H$_3$)$_2$), 19.5 (s, PCH(*C*H$_3$)$_2$), 19.4 (vt, *N* = 9.4, PCH(*C*H$_3$)$_2$), 16.6 (s, PCH(*C*H$_3$)$_2$). ^{31}P$\{^1$H$\}$ NMR (121.49 MHz, C_6D_6, 293K): δ 36.0 (s). ^{11}B NMR (96.29 MHz, C_6D_6, 293K): δ 52.0 (br).

Synthesis of OsHCl(η^2-H-Bpin)$\{\kappa^3$-*P*,*O*,*P*-[xant(P^{i}Pr$_2$)$_2$]} (5). To a suspension of [(Os(H···H)$\{\kappa^3$-*P*,*O*,*P*-[xant(P^{i}Pr$_2$)$_2$]$\}_2(\mu$-Cl)$_2][BF_4]_2$ (**3**) (51 mg; 0.034 mmol) in CH_2Cl_2 (3 mL) was added HBpin (25 µl; 0.172 mmol). After 10 min, the colorless solution obtained was taken to dryness. Addition of pentane (1mL) to the residue allowed the precipitation of a white solid, which was washed twice with pentane (2 mL) and dried under vacuum. Yield: 30 mg (54 %). Colorless crystals suitable for X-ray diffraction analysis were obtained by vapor diffusion of pentane into a toluene solution of the complex. Anal. Calcd. for $C_{33}H_{54}BClO_3OsP_2$: C, 49.72; H, 6.83. Found: C, 49.83; H, 6.69. HRMS (electrospray, m/z): calcd. for $C_{33}H_{54}BClO_3NaOsP_2$ $[M + Na]^+$: 821.2833, found: 821.2833. HRMS (electrospray, m/z): calcd. for $C_{33}H_{54}BO_3OsP_2$ $[M - Cl]^+$: 763.3258, found: 763.3261. ^{1}H NMR (300.13 MHz, C_6D_6, 293K): δ 7.25 (m, 2H, C*H*-arom), 7.06 (dd, $^3J_{HH}$ = 7.6, $^4J_{HH}$ = 1.6, 2H, C*H*-arom), 6.93 (dd, $^3J_{HH}$ = 7.6, $^3J_{HH}$ = 7.4, 2H, C*H*-arom), 3.03 (m, 2H, PC*H*(CH$_3$)$_2$), 2.90 (m, 2H, PC*H*(CH$_3$)$_2$), 1.75 (dvt, $^3J_{HH}$ = 7.1, *N* = 14.7, 6H, PCH(C*H*$_3$)$_2$), 1.62 (dvt, $^3J_{HH}$ = 7.1, *N* = 17.0, 6H, PCH(C*H*$_3$)$_2$), 1.35 (s, 3H, C*H*$_3$), 1.18 (s, 12H, C*H*$_3$ Bpin), 1.06 (s, 3H, C*H*$_3$), 1.06 (m, 6H, PCH(C*H*$_3$)$_2$), 1.10 (m, 6H, PCH(C*H*$_3$)$_2$), -12.99 (t, $^2J_{HP}$ = 11.0, 1H, Os*H*), -16.99 (br, 1H, Os(η^2-*H*-Bcat)). ^{13}C$\{^1$H$\}$-APT NMR (75.48 MHz, C_6D_6, 293K): δ 159.3 (vt, *N* = 12.5, *C*-arom), 132.6 (vt, *N* = 5.4, *C*-arom), 131.2 (s, *C*H-arom), 127.4 (vt, *N* = 26.1, *C*-arom), 127.0 (s, *C*H-arom), 124.8 (vt, *N* = 4.9, *C*H-arom), 82.4 (s, *C* Bpin), 35.6 (s, C(*C*H$_3$)$_2$), 34.4 (s, *C*(CH$_3$)$_2$), 27.6 (vt, *N* = 29.2, P*C*H(CH$_3$)$_2$), 25.8 (vt, *N* = 24.5, P*C*H(CH$_3$)$_2$), 25.1 (s, C(*C*H$_3$)$_2$), 24.9 (s, *C*H$_3$ Bpin), 21.4 (s, PCH(*C*H$_3$)$_2$), 19.9 (s, PCH(*C*H$_3$)$_2$), 19.8 (vt, *N* = 10.0, PCH(*C*H$_3$)$_2$), 16.9 (s, PCH(*C*H$_3$)$_2$). ^{31}P$\{^1$H$\}$ NMR (121.49 MHz, C_6D_6, 293K): δ 35.6 (s). ^{11}B NMR (96.29 MHz, C_6D_6, 293K): δ 46.5 (br).

Synthesis of OsH$_2$(η^2-H-Bcat)$\{\kappa^3$-*P*,*O*,*P*-[xant(P^{i}Pr$_2$)$_2$]} (7). HBcat (44 µl; 0.400 mmol) was added to a solution of $OsH_4\{\kappa^3$-*P*,*O*,*P*-[xant(P^{i}Pr$_2$)$_2$]} (**6**) (230 mg; 0.360 mmol) in C_6H_6 (3 mL). After 15 min stirring, the solvent was evaporated and pentane (1 mL) was added to afford a white solid which was washed once with pentane (1 mL) and dried under reduced pressure. Yield: 221 mg (80 %). Colorless crystals suitable for X-ray diffraction analysis were obtained by vapor diffusion of pentane into a toluene solution of the complex. Anal. Calcd. for $C_{33}H_{47}BO_3OsP_2$: C, 52.52; H, 6.28. Found: C, 52.74; H, 6.32. HRMS (electrospray, m/z): calcd. for $C_{33}H_{47}BO_3OsP_2$ $[M]^+$: 755.2632, found: 755.2651. ^{1}H NMR (300.13 MHz, C_6D_6, 298K): δ 7.26 (m, 2H, C*H*-arom), 7.11 (m, 2H, C*H*-arom Bcat), 6.89 (m, 4H, C*H*-arom), 6.82 (m, 2H, C*H*-arom Bcat), 3.24 (m, 2H, PC*H*(CH$_3$)$_2$), 2.37 (m, 2H, PC*H*(CH$_3$)$_2$), 1.44 (dvt, $^3J_{HH}$ = 7.9, *N* = 16.6, 6H, PCH(C*H*$_3$)$_2$), 1.30 (s, 3H, C*H*$_3$), 1.21 (m. 18H, PCH(C*H*$_3$)$_2$,), 0.93 (s, 3H, C*H*$_3$), -1.87 (br, 1H, Os*H*), -12.23 (br, 2H, Os*H*). ^{1}H NMR (400 MHz, C_7D_8, 193K): δ -1.90 (br, 1H, Os*H*), -5.60 (br, 1H, Os*H*), -18.83 (br, 1H, Os*H*). ^{13}C$\{^1$H$\}$-APT NMR (100.62 MHz, C_7D_8, 298K): δ 161.9 (vt, *N* = 13.7, *C*-arom), 153.1 (s, *C* Bcat), 133.2 (vt, *N* = 5.4, *C*-arom), 129.6 (s, *C*H-arom), 127.6 (vt, *N* = 25.5, *C*-arom), 125.4 (s, *C*H-arom), 125.2 (vt, *N* = 4.5, *C*H-arom), 120.1 (s, *C*H-arom Bcat), 110.0 (s, *C*H-arom Bcat), 34.7 (s, *C*(CH$_3$)$_2$), 33.7 (s, C(*C*H$_3$)$_2$), 27.4 (vt, *N* = 23.5, P*C*H(CH$_3$)$_2$), 23.0 (vt, *N* = 31.6, P*C*H(CH$_3$)$_2$), 22.8 (s, C(*C*H$_3$)$_2$), 20.3 (s, PCH(*C*H$_3$)$_2$), 19.7 (vt, *N* = 11.1, PCH(*C*H$_3$)$_2$), 19.2 (vt, *N* = 11.1, PCH(*C*H$_3$)$_2$), 16.7 (s, PCH(*C*H$_3$)$_2$). ^{31}P$\{^1$H$\}$ NMR (161.98 MHz, C_7D_8, 298K): δ 56.0 (s). ^{11}B NMR (96.29 MHz, C_7D_8, 298K): δ 45.5 (br).

Reaction of $OsH_4\{\kappa^3$-*P*,*O*,*P*-[xant(P^{i}Pr$_2$)$_2$]} with ClBcat. In a nmr tube, a solution of ClBcat (5 mg; 0.032 mmol) in C_6D_6 (0.6 mL) was added to $OsH_4\{\kappa^3$-*P*,*O*,*P*-[xant(P^{i}Pr$_2$)$_2$]} (**6**; 0.041 mg; 0.064 mmol). Immediate quantitative formation of a 1:1 mixture of complexes $OsH_2(\eta^2$-H-Bcat)$\{\kappa^3$-*P*,*O*,*P*-[xant(P^{i}Pr$_2$)$_2$]} (**7**) and $OsH_3Cl\{\kappa^3$-*P*,*O*,*P*-[xant(P^{i}Pr$_2$)$_2$]} (**1**) was observed according to NMR measurements.

Computational Details and Cartesian Coordinates of 4, 5, and 7. Geometry optimizations were performed without symmetry constraints using the Gaussian09[25] suite of programs at the BP86[26]/def2-SVP[27] level of theory using the D3 dispersion correction suggested by Grimme et al.[28] This level is denoted BP86-D3/def2-SVP. Complexes **4**, **5** and **7** were characterized by frequency calculations, and have positive definite Hessian matrices thus confirming that the computed structures are minima on the potential energy surface. WBIs have been computed using the NBO method.[29]

All AIM results described in this work correspond to calculations performed at the BP86-D3/6-31+G(d)/WTBS(for Os) level on the optimized geometry obtained at the BP86-D3/def2-SVP level. The WTBS (well-tempered basis sets)[30] have been recommended for AIM calculations involving transition metals.[31] The topology of the electron density was conducted using the AIMAll program package.[32]

The interaction between the transition metal fragment and the borane and HBcat in complexes **4** and **7** has been investigated with the EDA-NOCV method,[33] which combines the energy decomposition analysis (EDA)[34] with the natural orbitals for chemical valence (NOCV)[35] methods. Within this approach, the interaction energy can be decomposed into the following physically meaningful terms:

$\Delta E_{int} = \Delta E_{elstat} + \Delta E_{Pauli} + \Delta E_{orb} + \Delta E_{disp}$

The term ΔE_{elstat} corresponds to the classical electrostatic interaction between the unperturbed charge distributions of the deformed reactants and is usually attractive. The Pauli repulsion ΔE_{Pauli} comprises the destabilizing interactions between occupied orbitals and is

responsible for any steric repulsion. The orbital interaction ΔE_{orb} accounts for charge transfer (interaction between occupied orbitals on one moiety with unoccupied orbitals on the other, including HOMO–LUMO interactions) and polarization (empty-occupied orbital mixing on one fragment due to the presence of another fragment). Finally, the ΔE_{disp} term takes into account the interactions which are due to dispersion forces.

The EDA-NOCV method makes it possible to further partition the total orbital interactions into pairwise contributions of the orbital interactions. Details of the method can be found in the literature.[36]

The EDA-NOCV calculations were carried out using the BP86-D3/def2-SVP optimized geometries with the program package ADF 2016.01 using the same functional (BP86-D3) in conjunction with a triple-ζ-quality basis set using uncontracted Slater-type orbitals (STOs) augmented by two sets of polarization function with a frozen-core approximation for the core electrons. An auxiliary set of s, p, d, f, and g STOs were used to fit the molecular densities and to represent the Coulomb and exchange potentials accurately in each SCF cycle.[37] Scalar relativistic effects were incorporated by applying the zeroth-order regular approximation (ZORA).[38] This level of theory is denoted BP86-D3/TZ2P//BP86-D3/def2-SVP.

Structural Analysis of Complexes 4, 5, and 7. The cif files of **4**, **5**, and **7** have been deposited with the Cambridge Crystallographic Data Center (Nos. CCDC 1552854 (**4**), CCDC 1552855 (**5**), and CCDC 1552856 (**7**)). X-ray data were collected for the complexes on a Bruker Smart APEX DUO (**5**) or Bruker Smart APEX CCD (**4**, **7**) diffractometers equipped with a normal focus, 2.4 kW sealed tube source (Mo radiation, λ = 0.71073 Å) operating at 50 kV and 40 mA (**4**) or 30 mA (**5** and **7**). Data were collected over the complete sphere. Each frame exposure time was 10 s (**5** and **7**), or 20 s (**4**) covering 0.3° in ω. Data were corrected for absorption by using a multiscan method applied with the SADABS program.[39] The structures were solved by Patterson or direct methods and refined by full-matrix least squares on F^2 with SHELXL2016,[40] including isotropic and subsequently anisotropic displacement parameters. The hydrogen atoms were observed in the least Fourier Maps or calculated, and refined freely or using a restricted riding model. The hydrogen bonded to metal atoms were observed in the last cycles of refinement but refined too close to metals, so a restricted refinement model was used for all of them (d(Os-H = 1.59(1) Å).

Crystal data for **4**: $C_{33}H_{46}BClO_3OsP_2$, 2(CH_2Cl_2), M_W 958.95, colourless, irregular block (0.238 x 0.188 x 0.082), triclinic, space group P-1, *a*: 11.8674(6) Å, *b*: 16.6502(8) Å, *c*: 20.7567(10) Å, *α*: 104.9620(10)°, *β*: 96.3580(10)°, *γ*: 90.0110(10)°, *V* = 3936.2(3) Å^3, *Z* = 4, *Z'* = 2, D_{calc}: 1.618 g cm^{-3}, F(000): 1920, T = 100(2) K, μ 3.694 mm^{-1}. 67147 measured reflections (2θ: 3-58°, ω scans 0.3°), 18814 unique (R_{int} = 0.0368); min./max. transm. Factors 0.659/0.862. Final agreement factors were R^1 = 0.0287 (15471 observed reflections, I > 2σ(I)) and wR^2 = 0.0659; data/restraints/parameters 18814/8/881; GoF = 0.998. Largest peak and hole 1.169 (close to osmium atom) and -1.063 e/ Å^3.

Crystal data for **5**: $C_{33}H_{54}BClO_3OsP_2$, M_W 797.16, colourless, irregular block (0.191 x 0.185 x 0.134), orthorhombic, space group Pnma, *a*: 18.7529(17) Å, *b*: 18.1959(17) Å, *c*: 10.5608(10)Å, *V* = 3603.6(6) Å^3, *Z* = 4, *Z'* = 0.5, D_{calc}: 1.469 g cm^{-3}, F(000): 1616, T = 100(2) K, μ 3.731 mm^{-1}. 39075 measured reflections (2θ: 3-58°, ω scans 0.3°), 5004 unique (R_{int} = 0.0291); min./max. transm. Factors 0.739/0.862. Final agreement factors were R^1 = 0.0161 (4661 observed reflections, I > 2σ(I)) and wR^2 = 0.0424; data/restraints/parameters 5004/14/235; GoF = 0.998. Largest peak and hole 0.883 (close to osmium atoms) and -0.756 e/ Å^3.

Crystal data for **7**: $C_{33}H_{47}BO_3OsP_2$, M_W 754.65, colourless, irregular block (0.261 x 0.186 x 0.160), orthorhombic, space group Pna21, *a*: 19.3235(11) Å, *b*: 19.7359(11) Å, *c*: 8.6538(5) Å, *V* = 3300.3(3) Å^3, *Z* = 4, *Z'* = 1, D_{calc}: 1.519 g cm^{-3}, F(000): 1520, T = 100(2) K, μ 3.992 mm^{-1}. 31075 measured reflections (2θ: 3-57°, ω scans 0.3°), 7781 unique (R_{int} = 0.0284); min./max. transm. Factors 0.601/0.746. Final agreement factors were R^1 = 0.0193 (7372 observed reflections, I > 2σ(I)) and wR^2 = 0.0513; data/restraints/parameters 7781/3/381; GoF = 0.795. Largest peak and hole 0.806 (close to osmium atoms) and -0.644 e/ Å^3.

ASSOCIATED CONTENT

Supporting Information

The Supporting Information is available free of charge on the ACS Publications website.

NMR spectra and Total energies of **4**, **5** and **7**. (PDF)

Theoretical complex coordinates. (XYZ)

AUTHOR INFORMATION

Corresponding Author

*E-mail for M.A.E.: maester@unizar.es

Notes

The authors declare no competing financial interest.

ACKNOWLEDGMENT

Financial support from MINECO of Spain (Projects CTQ2013-44303-P, CTQ2014-52799-P, CTQ2016-78205-P and CTQ2016-81797-REDC), Diputación General de Aragón (E35), FEDER, and European Social Fund is acknowledged.

REFERENCES

(1) Esteruelas, M. A.; López, A. M.; Oliván, M. *Chem. Rev.* **2016**, *116*, 8770-8847.

(2) (a) Kubas, G. J. *Metal Dihydrogen and σ-Bond Complexes: Structure, Theory and Reactivity*; Kluwer: New York, 2001. (b) Kubas, G. J. *J. Organomet. Chem.* **2001**, *635*, 37-68. (c) Kubas, G. J. *Chem. Rev.* **2007**, *107*, 4152-4205. (d) Kubas, G. J. *J. Organomet. Chem.* **2014**, *751*, 33-49. (e) Crabtree, R. H. *Chem. Rev.* **2016**, *116*, 8750-8769.

(3) (a) Lin, Z. Y. *Chem. Soc. Rev.* **2002**, *31*, 239-245. (b) Lachaize, S.; Sabo-Etienne, S. *Eur. J. Inorg. Chem.* **2006**, 2115-2127. (c) Perutz, R. N.; Sabo-Etienne, S. *Angew. Chem., Int. Ed.* **2007**, *46*, 2578-2592.

(4) (a) Miyaura, N. *Bull. Chem. Soc. Jpn.* **2008**, *81*, 1535-1553. (b) Crudden, C. M.; Glasspoole, B. W.; Lata, C. J. *Chem. Commun.* **2009**, 6704-6716. (c) Dang, L.; Lin, Z. Y.; Marder, T. B. *Chem. Commun.* **2009**, 3987-3995. (d) Mkhalid, I. A. I.; Barnard, J. H.; Marder, T. B.; Murphy, J. M.; Hartwig, J. F. *Chem. Rev.* **2010**, *110*, 890-931. (e) Ros, A.; Fernández, R.; Lassaletta, J. M. *Chem. Soc. Rev.* **2014**, *43*, 3229-3243.

(5) (a) Hamilton, C. W.; Baker, R. T.; Staubitz, A.; Manners, I. *Chem. Soc. Rev.* **2009**, *38*, 279-293. (b) Waterman, R. *Chem. Soc. Rev.* **2013**, *42*, 5629-5641. (c) St John, A.; Goldberg, K. I.; Heinekey, D. M. *Top. Organomet. Chem.* **2013**, *40*, 271-287. (d) Rossin, A.; Peruzzini, M. *Chem. Rev.* **2016**, *116*, 8848-8872. (e) Bhunya, S.; Malakar, T.; Ganguly, G.; Paul, A. *ACS Catal.* **2016**, *6*, 7907-7934.

(6) Pandey, K. K. *Coord. Chem. Rev.* **2009**, *253*, 37-55.

(7) (a) Hartwig, J. F.; Muhoro, G. N.; He, X. M.; Eisenstein, O.; Bosque, R.; Maseras, F. *J. Am. Chem. Soc.* **1996**, *118*, 10936-10937. (b) Muhoro, C. N.; Hartwig, J. F. *Angew. Chem., Int. Ed. Engl.* **1997**, *36*, 1510-1512. (c) Muhoro, C. N.; He, X. M.; Hartwig, J. F. *J. Am. Chem. Soc.* **1999**, *121*, 5033-5046. (d) Lam, W. H.; Lin, Z. Y. *Organometallics* **2000**, *19*, 2625-2628.

(8) Schlecht, S.; Hartwig, J. F. *J. Am. Chem. Soc.* **2000**, *122*, 9435-9443.

(9) Crestani, M. G.; Muñoz-Hernández, M.; Arévalo, A.; Acosta-Ramírez, A.; García, J. J. *J. Am. Chem. Soc.* **2005**, *127*, 18066-18073.

(10) (a) Montiel-Palma, V.; Lumbierres, M.; Donnadieu, B.; Sabo-Etienne, S.; Chaudret, B. *J. Am. Chem. Soc.* **2002**, *124*, 5624-5625. (b) Lachaize, S.; Essalah, W.; Montiel-Palma, V.; Vendier, L.; Chaudret, B.; Barthelat, J. C.; Sabo-Etienne, S. *Organometallics* **2005**, *24*, 2935-2943. (c) Alcaraz, G.; Grellier, M.; Sabo-Etienne, S. *Acc. Chem. Res.* **2009**, *42*, 1640-1649.

(11) Hebden, T. J.; Denney, M. C.; Pons, V.; Piccoli, P. M. B.; Koetzle, T. F.; Schultz, A. J.; Kaminsky, W.; Goldberg, K. I.; Heinekey, D. M. *J. Am. Chem. Soc.* **2008**, *130*, 10812-10820.

(12) (a) Esteruelas, M. A.; López, A. M.; Mora, M.; Oñate, E. *Chem. Commun.* **2013**, *49*, 7543-7545. (b) Esteruelas, M. A.; López, A. M.; Mora, M.; Oñate, E. *Organometallics* **2015**, *34*, 941-946.

(13) Hartwig, J. F.; Cook, K. S.; Hapke, M.; Incarvito, C. D.; Fan, Y. B.; Webster, C. E.; Hall, M. B. *J. Am. Chem. Soc.* **2005**, *127*, 2538-2552.

(14) Alcaraz, G.; Sabo-Etienne, S. *Coord. Chem. Rev.* **2008**, *252*, 2395-2409.

(15) (a) Pontiggia, A. J.; Chaplin, A. B.; Weller, A. S. *J. Organomet. Chem.* **2011**, *696*, 2870-2876. (b) Dallanegra, R.; Chaplin, A. B.; Weller, A. S. *Organometallics* **2012**, *31*, 2720-2728.

(16) (a) Pawley, R. J.; Moxham, G. L.; Dallanegra, R.; Chaplin, A. B.; Brayshaw, S. K.; Weller, A. S.; Willis, M. C. *Organometallics* **2010**, *29*, 1717-1728. (b) Esteruelas, M. A.; Honczek, N.; Oliván, M.; Oñate, E.; Valencia, M. *Organometallics* **2011**, *30*, 2468-2471. (c) Miloserdov, F. M.; Grushin, V. V. *Angew. Chem., Int. Ed.* **2012**, *51*, 3668-3672. (d) Alós, J.; Bolaño, T.; Esteruelas, M. A.; Oliván, M.; Oñate, E.; Valencia, M. *Inorg. Chem.* **2013**, *52*, 6199-6213. (e) Esteruelas, M. A.; Oliván, M.; Vélez, A. *Inorg. Chem.* **2013**, *52*, 12108-12119. (f) Johnson, H. C.; Leitao, E. M.; Whitten, G. R.; Manners, I.; Lloyd-Jones, G. C.; Weller, A. S. *J. Am. Chem. Soc.* **2014**, *136*, 9078-9093. (g) Alós, J.; Bolaño, T.; Esteruelas, M. A.; Oliván, M.; Oñate, E.; Valencia, M. *Inorg. Chem.* **2014**, *53*, 1195-1209. (h) Ren, P.; Pike, S. D.; Pernik, I.; Weller, A. S.; Willis, M. C. *Organometallics* **2015**, *34*, 711-723. (i) Esteruelas, M. A.; Oliván, M.; Vélez, A. *Organometallics* **2015**, *34*, 1911-1924. (j) Esteruelas, M. A.; Oliván, M.; Vélez, A. *J. Am. Chem. Soc.* **2015**, *137*, 12321-12329. (k) Esteruelas, M. A.; Nolis, P.; Oliván, M.; Oñate, E.; Vallribera, A.; Vélez, A. *Inorg. Chem.* **2016**, *55*, 7176-7181.

(17) Esteruelas, M. A.; García-Yebra, C.; Martín, J.; Oñate, E. *Inorg. Chem.* **2017**, *56*, 676-683.

(18) Buil, M. L.; Cardo, J. J. F.; Esteruelas, M. A.; Fernández, I.; Oñate, E. *Inorg. Chem.* **2016**, *55*, 5062-5070.

(19) Jessop, P. G.; Morris, R. H. *Coord. Chem. Rev.* **1992**, *121*, 155-284.

(20) (a) Irvine, G. J.; Roper, W. R.; Wright, L. J. *Organometallics* **1997**, *16*, 2291-2296. (b) Rickard, C. E. F.; Roper, W. R.; Williamson, A.; Wright, L. J. *Organometallics* **1998**, *17*, 4869-4874. (c) Rickard, C. E. F.; Roper, W. R.; Williamson, A.; Wright, L. J. *Angew. Chem., Int. Ed.* **1999**, *38*, 1110-1113. (d) Rickard, C. E. F.; Roper, W. R.; Williamson, A.; Wright, L. J. *Organometallics* **2000**, *19*, 4344-4355. (e) Irvine, G. J.; Rickard, C. E. F.; Roper, W. R.; Williamson, A.; Wright, L. J. *Angew. Chem., Int. Ed.* **2000**, *39*, 948-950. (f) Rickard, C. E. F.; Roper, W. R.; Williamson, A.; Wright, L. J. *Organometallics* **2002**, *21*, 1714-1718. (g) Rickard, C. E. F.; Roper, W. R.; Williamson, A.; Wright, L. J. *Organometallics* **2002**, *21*, 4862-4872. (h) Rickard, C. E. F.; Roper, W. R.; Williamson, A.; Wright, L. J. *J. Organomet. Chem.* **2004**, *689*, 1609-1616. (i) Buil, M. L.; Esteruelas, M. A.; Garcés, K.; Oñate, E. *J. Am. Chem. Soc.* **2011**, *133*, 2250-2263. (j) Esteruelas, M. A.; Fernández, I.; López, A. M.; Mora, M.; Oñate, E. *Organometallics* **2012**, *31*, 4646-4649. (k) Esteruelas, M. A.; López, A. M.; Mora, M.; Oñate, E. *Organometallics* **2012**, *31*, 2965-2970. (l) Buil, M. L.; Esteruelas, M. A.; Fernández, I.; Izquierdo, S.; Oñate, E. *Organometallics* **2013**, *32*, 2744-2752. (m) Braunschweig, H.; Légare, M. A.; Matler, A.; Wennemann, B. *Eur. J. Inorg. Chem.* **2016**, 3376-3379. (n) McQueen, C. M. A.; Hill, A. F.; Sharma, M.; Singh, S. K.; Ward, J. S.; Willis, A. C.; Young, R. D. *Polyhedron* **2016**, *120*, 185-195.

(21) Alós, J.; Esteruelas, M. A.; Oliván, M.; Oñate, E.; Puylaert, P. *Organometallics* **2015**, *34*, 4908-4921.

(22) $\Delta G/RT_c = 22.96 + Ln(T_c/\delta\nu)$.

(23) Morris, R. H. *Chem. Rev.* **2016**, *116*, 8588-8654.

(24) Bénac-Lestrille, G.; Helmstedt, U.; Vendier, L.; Alcaraz, G.; Clot, E.; Sabo-Etienne, S. *Inorg. Chem.* **2011**, *50*, 11039-11045.

(25) Frisch, M. J.; Trucks, G. W.; Schlegel, H. B.; Scuseria, G. E.; Robb, M. A.; Cheeseman, J. R.; Scalmani, G.; Barone, V.; Mennucci, B.; Petersson, G. A.; Nakatsuji, H.; Caricato, M.; Li, X.; Hratchian, H. P.; Izmaylov, A. F.; Bloino, J.; Zheng, G.; Sonnenberg, J. L.; Hada, M.; Ehara, M.; Toyota, K.; Fukuda, R.; Hasegawa, J.; Ishida, M.; Nakajima, T.; Honda, Y.; Kitao, O.; Nakai, H.; Vreven, T.; Montgomery, J. A., Jr.; Peralta, J. E.; Ogliaro, F.; Bearpark, M.; Heyd, J. J.; Brothers, E.; Kudin, K. N.; Staroverov, V. N.; Kobayashi, R.; Normand, J.; Raghavachari, K.; Rendell, A.; Burant, J. C.; Iyengar, S. S.; Tomasi, J.; Cossi, M.; Rega, N.; Millam, N. J.; Klene, M.; Knox, J. E.; Cross, J. B.; Bakken, V.; Adamo, C.; Jaramillo, J.; Gomperts, R.; Stratmann, R. E.; Yazyev, O.; Austin, A. J.; Cammi, R.; Pomelli, C.; Ochterski, J. W.; Martin, R. L.; Morokuma, K.; Zakrzewski, V. G.; Voth, G. A.; Salvador, P.; Dannenberg, J. J.; Dapprich, S.; Daniels, A. D.; Farkas, Ö.; Foresman, J. B.; Ortiz, J. V.; Cioslowski, J.; Fox, D. J. Gaussian 09, Revision B.01; Gaussian, Inc.: Wallingford, CT, 2009.

(26) Zhao, Y.; Schultz, N. E.; Truhlar, D. G. *J. Chem. Theory Comput.* **2006**, *2*, 364-382.

(27) Weigend, F.; Ahlrichs, R. *Phys. Chem. Chem. Phys.* **2005**, *7*, 3297-3305.

(27) Grimme, S.; Antony, J.; Ehrlich, S.; Krieg, H. *J. Chem. Phys.* **2010**, *132*.

(29) (a) Foster, J. P.; Weinhold, F. *J. Am. Chem. Soc.* **1980**, *102*, 7211-7218. (b) Reed, A. E.; Weinhold, F. *J. Chem. Phys.* **1985**, *83*, 1736-1740. (c) Reed, A. E.; Weinstock, R. B.; Weinhold, F. *J. Chem. Phys.* **1985**, *83*, 735-746. (d) Reed, A. E.; Curtiss, L. A.; Weinhold, F. *Chem. Rev.* **1988**, *88*, 899-926.

(30) (a) Huzinaga, S.; Miguel, B. *Chem. Phys. Lett.* **1990**, *175*, 289-291. (b) Huzinaga, S.; Kolbukowski, M. *Chem. Phys. Lett.* **1993**, *212*, 260-264.

(31) Cabeza, J. A.; Van der Maelen, J. F.; García-Granda, S. *Organometallics* **2009**, *28*, 3666-3672 and references therein.

(31) Keith, T. A., AIMA11, 2010, http://tkgristmill.com

(33) Mitoraj, M. P.; Michalak, A.; Ziegler, T. *J. Chem. Theory Comput.* **2009**, *5*, 962-975.

(34) For a recent review see: von Hopffgarten, M.; Frenking, G. *Wiley Interdisciplinary Reviews-Computational Molecular Science* **2012**, *2*, 43-62.

(34) Mitoraj, M.; Michalak, A. *J. Mol. Model.* **2007**, *13*, 347-355.

(36) See for instance: (a) Mitoraj, M. P.; Michalak, A.; Ziegler, T. *Organometallics* **2009**, *28*, 3727-3733. (b) Thi, A. N. N.; Frenking, G. *Chem. Eur. J.* **2012**, *18*, 12733-12748. (c) Parafiniuk, M.; Mitoraj, M. P. *Organometallics* **2013**, *32*, 4103-4113. (d) Mondal, K. C.; Samuel, P. P.; Roesky, H. W.; Carl, E.; Herbst-Irmer, R.; Stalke, D.; Schwederski, B.; Kaim, W.; Ungur, L.; Chibotaru, L. F.; Hermann, M.; Frenking, G. *J. Am. Chem. Soc.* **2014**, *136*, 1770-1773.

(37) Krijn, A.; Baerends, E. J.; Fit Functions in the HFS-Method, Internal Report (in Dutch), Vrije Universiteit Amsterdam, The Netherlands, **1984**.

(38) (a) van Lenthe, E.; Baerends, E. J.; Snijders, J. G. *J. Chem. Phys.* **1993**, *99*, 4597-4610. (b) van Lenthe, E.; Baerends, E. J.; Snijders, J. G. *J. Chem. Phys.* **1994**, *101*, 9783-9792. (c) van Lenthe, E.; Ehlers, A.; Baerends, E. J. *J. Chem. Phys.* **1999**, *110*, 8943-8953.

(39) Blessing, R. H. *Acta Cryst.* **1995**, A*51*, 33-38. SADABS: Area-detector absortion correction; Bruker-AXS, Madison, WI, **1996**.

(40) SHELXL-2016/6. Sheldrick, G. M. *Acta Cryst.* **2008**, *A64*, 112-122.

Table of Contents

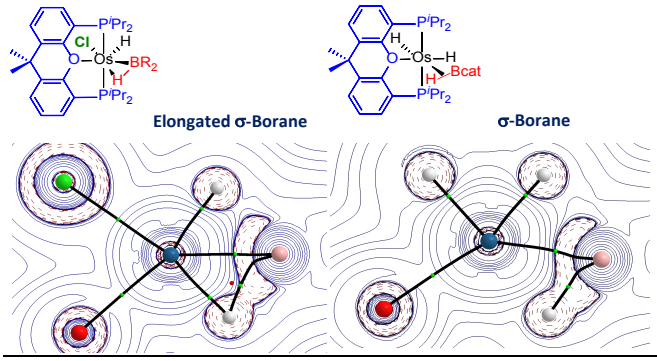
Elongated σ-Borane
σ-Borane